Sintering of Au Particles Supported on TiO_2(110) during CO Oxidation

F. Yang, M. S. Chen, and D. W. Goodman*

Department of Chemistry, Texas A&M University, P.O. Box 30012, College Station, Texas 77842-3012

Received: September 4, 2008; Revised Manuscript Received: November 3, 2008

Sintering of supported metal catalysts is of primary interest in heterogeneous catalysis. The presence of reactant gases, especially oxidants, often accelerates the sintering of supported metal catalysts. Our in situ studies using scanning tunneling microscopy (STM) compare the sintering of Au particles supported on TiO_2(110) in the presence of CO, O_2, or mixtures of the two gases. The results reveal a synergetic effect of CO/O_2 mixtures in accelerating the sintering of supported Au particles. By monitoring the morphological changes of individual Au particles, in situ studies allow investigation of the sintering kinetics of Au particles supported on TiO_2(110) during CO oxidation. The results support a reactant-induced mechanism and provide a more complete kinetic description of the sintering of supported metal catalysts beyond a mean-field description.

Introduction

Sintering of metal particles supported on oxide surfaces is a central theme of catalytic research. Metal particles of several nanometers in size, supported on oxide surfaces, are often efficient catalysts.[1−6] These catalysts, however, frequently deactivate as the average size of the supported metal particles increases via sintering.[7−9] For example, Au particles in the 2−4 nm size range supported on high-surface-area titania exhibit a remarkable catalytic reactivity for low temperature CO oxidation and selective hydrogenation reactions.[1−6,8,10] Although supported Au catalysts have great potential in technological applications, for example, removing CO that poisons fuel cell catalysts, a major problem for the commercialization of supported Au catalysts is that these catalysts deactivate rapidly.[8,9,11] Similar deactivation has been observed for model catalysts consisting of Au particles deposited on a reduced TiO_2(110) where rapid deactivation has been shown to correlate with sintering of the Au particles.[9,12] The underlying mechanism for the sintering of supported Au particles during CO oxidation remains unclear. To understand the sintering of supported Au catalysts, we have studied the sintering kinetics of Au/TiO_2(110) during CO oxidation and have compared these kinetics with the kinetics found in the presence of CO or O_2 alone.

The first issue in sintering kinetics is to determine the primary mass transport process. The sintering of supported nanoparticles can occur in either one or two modes: (i) the migration and coalescence of whole particles; or (ii) the migration of monomers (single metal atoms or metal complexes). The first mode, known as particle migration, entails the migration of whole particles on the surface, which then coalesce with neighboring particles. In the second mode, known as Ostwald ripening, monomers dissociate from small particles, diffuse to, and then coalesce with large particles. Kinetic models of the sintering of supported metal particles have been developed on the basis of these two modes.[13,14]

Previous experimental studies[7,15] have attempted to determine the predominant mass transport mode, as well as the kinetic parameters of sintering, by fitting the average particle size distribution or average particle size with theoretical kinetic models. These models apply the rate equation of sintering for a single particle, which are then generalized with approximations to particles over the entire distribution. On the other hand, previous kinetic studies have focused on the behavior of the entire ensemble or particles, such as average particle dispersion and average particle size, rather than on individual particles. Discrepancies remain between the kinetics predicted by these theoretical models and experimental results on the sintering of supported metal particles.[15,16]

An in situ scanning tunneling microscope (STM) allows one to monitor individual particles under realistic conditions and to determine directly the mass transport mode controlling the kinetics. Continuous STM snapshots of individual particles can reveal which mode dominates the sintering process. Moreover, STM measurements on the metal particle volume and the change in this volume as a function of time at constant temperature can provide very precise rate data for the simulation of sintering kinetics and the determination of the activation energy of sintering.

In situ STM studies on metal particles supported on oxide surfaces are scarce, especially at elevated pressures and temperatures,[17−19] due to experimental difficulties related to tip instability in the reactive environment and scan drifts caused by ambient pressure/temperature changes. Methods to overcome these difficulties have been addressed in previous studies.[18−20] In this Article, we report an in situ kinetic study on the sintering of Au particles supported on TiO_2(110) during CO oxidation. To our knowledge, this is the first kinetic study that directly measures the sintering kinetics of a supported model catalyst.

Experimental Section

The experiments were performed in a STM chamber, which can be pressurized to 1 atm. The STM chamber was attached to a UHV analysis chamber equipped with Auger electron spectroscopy (AES) and mass spectroscopy (MS). The base pressures of both chambers are $<3 \times 10^{-10}$ Torr. The STM is a commercial variable temperature STM (RHK VT-UHV-300). A 30 W halogen lamp was used for heating the sample while the STM images were acquired at elevated temperatures and pressures.

A TiO_2(110) single crystal (Princeton Scientific) was cleaned by repeated cycles of Ar ion sputtering and vacuum annealing

* Corresponding author. Tel.: (979) 845-0214. Fax: (979) 845-6822. E-mail: goodman@mail.chem.tamu.edu.

10.1021/jp807865w CCC: $40.75 © 2009 American Chemical Society
Published on Web 12/10/2008

to 1000 K; the cleaned TiO_2(110) surface exhibited a (1 × 1) surface structure. Au was evaporated onto the TiO_2(110) surface by resistive heating a W filament wrapped with high purity Au wire. Both CO and O_2 were ultrahigh purity (UHP) grade and were further purified using liquid N_2 before they were backfilled into the STM chamber. Electrochemically etched W tips, Au tips, and Au-coated Pt−Ir tips were used in this study. Au tips and Au-coated Pt−Ir tips exhibited excellent chemical inertness in O_2 or during CO oxidation, while W tips were used mainly for imaging in the presence of CO.

To reduce the tip influence of surface dynamical processes, scanning parameters were selected to ensure large tip surface separation (∼20 GΩ). The scanning parameters were fixed to minimize changes in the apparent size of the Au particles. The bias was held at 2 V, and the current was fixed at 0.1 nA. With consideration of the stability of the tunnel junctions, images were acquired at a rate of 5−7 min/frame in the constant current mode. STM images were acquired on the same region of the surface, enabling the sintering of individual particles to be followed.

Results and Discussion

The sintering of Au/TiO_2(110) during CO oxidation was studied between 300 and 410 K with a total gas pressure of 0.1 Torr and a CO/O_2 gas mixture of 1:1. Figure 1 shows the morphological changes of 0.5 ML Au particles supported on TiO_2(110) in the presence of CO/O_2 at 300 K. Under UHV conditions, the Au particles remain immobile and show no detectable change of either particle size or shape for more than 4 h. Sintering of Au particles began immediately upon the introduction of a 0.1 Torr CO/O_2 gas mixture (1:1 ratio). Consecutive images were then acquired on the same surface area as a function of time. Figure 1 shows no apparent change of particle positions before and after gas exposure; however, the small Au particles gradually decayed, whereas the large Au particles grew in size. The gradual change of the particle size and static particle positions are consistent with an Ostwald ripening process. As captured in the series of images, Au particles with a height around 2.3 Å disappeared within 28 min after introduction of the gas mixture. Most Au particles with a height around 4.6 Å or less (assuming the height of Au particles of 2 layer thickness is 4.6 Å[21]) disappeared within 2 h of CO oxidation reaction. The number density of the Au particles decreased from 1.6×10^{12} to $6.9 \times 10^{11}/cm^2$ after 2 h of CO oxidation, and then decreased slowly thereafter.

Figure 2 shows the sintering of 0.2 ML Au/TiO_2(110) in the presence of 0.1 Torr CO/O_2 at 300 K. Similar to Figure 1, large Au particles grew at the expense of small Au particles, with no apparent change in the particle position. Most Au particles with a height of 4.6 Å or less disappeared within 2 h of CO oxidation. The density of the Au particles decreased from 1.5×10^{12} to $7.1 \times 10^{11}/cm^2$ within 2 h, and then decreased slowly thereafter.

At elevated temperatures, CO oxidation-induced sintering of supported Au particles was observed at an increased sintering rate. Figure 3 summarizes the morphological changes of 0.65 ML Au/TiO_2(110) at 410 K in 0.1 Torr CO/O_2. Similar to Figure 1, Au particles were found to sinter via Ostwald ripening. Most Au particles with a height less than 4.6 Å disappeared within 1 h of CO oxidation reaction. The total particle density decreased by 60% to $6.9 \times 10^{11}/cm^2$ within 1 h of CO oxidation and slowly decreased thereafter. An adsorbate-induced change of the substrate morphology became apparent at elevated temperatures. The density of small protrusions with a height around 1−2 Å increased during the reaction. These protrusions are believed

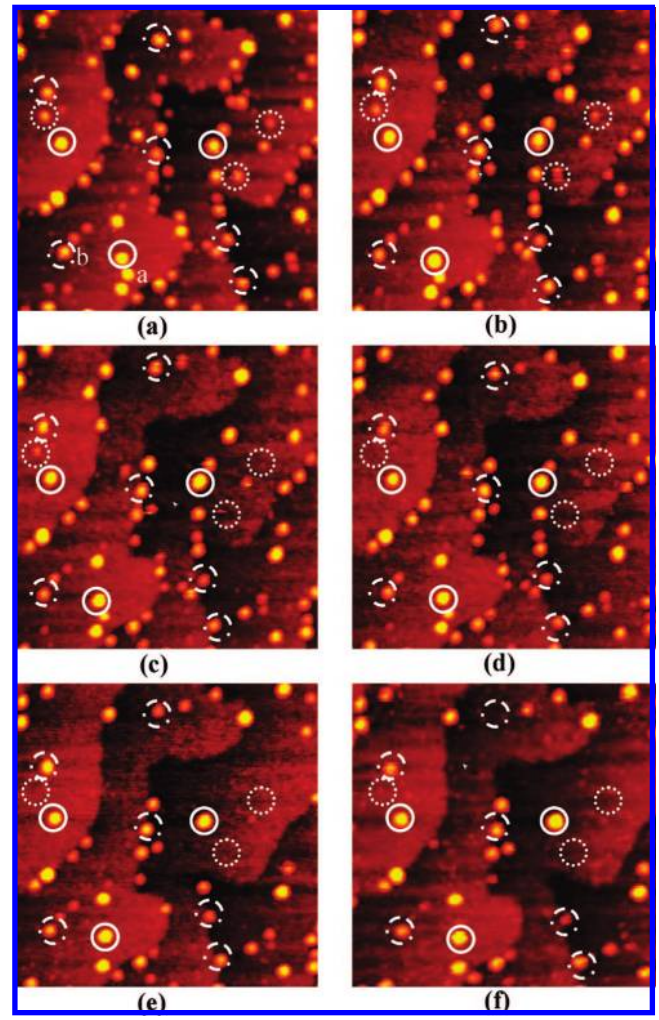

Figure 1. 75 × 75 nm^2 in situ STM images of 0.5 ML Au particles supported on the TiO_2(110) surface in the presence of 0.1 Torr CO and O_2 mixture at 300 K. (a−f) STM subsequently acquired of the same surface region. The time intervals following introduction of the reactants were (a) 0 min; (b) 28 min; (c) 42 min; (d) 63 min; (e) 120 min; and (f) 280 min. Examples of Au particles that decay/grow are marked with dotted/solid circles, respectively. To show the local effect, dashed circles mark Au particles of similar size, but with different decay rates. Depending on their local environment, a larger Au particle (a) can decay, while the smaller Au particle (b) grows.

to be TiO_x species formed on the TiO_2(110) surface during CO oxidation. The formation of TiO_x has been observed in the surface reoxidation of TiO_2(110).[22,23] In the presence of oxygen, interstitial Ti ions diffuse to the surface and form TiO_x, which can then serve as a precursor to surface regrowth. These protrusions are not likely to be small Au atoms because Au particles of monolayer thickness are unstable and decay rapidly in the presence of 0.1 Torr CO/O_2, as shown in Figure 1.

Figure 4 compares the height distribution of Au particles before and after 2 h of CO oxidation at 300 and 410 K. The number density of Au particles with height greater than the median height increases, whereas the number density of Au particles with height smaller than the median height decreases. For Au particles of the same size, the decay rates of Au particles increase as the surface temperature or the surface coverage is increased. The sintering of Au particles with height less than 4.6 Å is very rapid and less influenced by the surface Au coverage. For Au particles with varying coverages, in the presence of 0.1 Torr CO/O_2, the decrease in the particle density

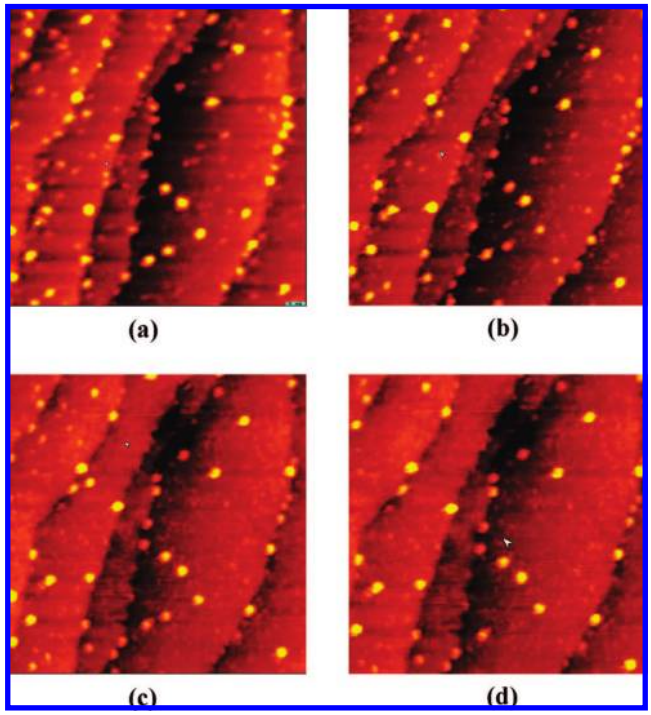

Figure 2. 75 × 75 nm^2 in situ STM images of 0.2 ML Au particles supported on the TiO_2(110) surface in the presence of 0.1 Torr CO and O_2 mixture gas at 300 K. (a−d) STM images subsequently acquired of the same surface region. The time intervals following introduction of the reactants were (a) 0 min; (b) 21 min; (c) 63 min; and (d) 120 min.

becomes less apparent after the total particle density falls to approximately 7 × 10^{11}/cm^2.

Au particles supported on TiO_2(110) were also exposed to O_2 and CO separately to investigate the influence of the chemisorbed reactants. The influence of O_2 exposure is shown in Figure 5a and b. Minimal changes were observed for 0.5 ML Au particles supported on TiO_2(110) after an exposure of 0.1 Torr O_2 for 1.5 h at 300 K. In contrast to the rapid sintering observed during CO oxidation, most Au particles with a height above 2.3 Å remain. The number density of Au particles was 1.5 × 10^{12}/cm^2 after O_2 exposure, more than twice the density after CO oxidation. Au particles of one monolayer thickness were not stable in O_2 and disappeared after an exposure to 0.1 Torr O_2. No change in the particle positions was evident, and no growth of new particles was observed. The influence of CO exposure on 0.5 ML Au particles supported on TiO_2(110) is compared in Figure 5c and d. The exposure of 3 Torr CO at 300 K did not result in any noticeable change in either the TiO_2 substrate or the supported Au particles for 2 h. Comparing Figures 1 and 5, a synergetic effect of CO/O_2 was found to induce and accelerate the sintering of Au particles on TiO_2(110).

Adsorbate-induced changes in the surface morphology have been observed extensively for supported metal particles.[9,15,17,18,24−31] For example, CO and NO have been reported to promote the dissociation of Rh and Ir particles into metal atoms at room temperature.[29,30,32−34] At relatively high temperatures (>600 °C), accelerated sintering of supported metal catalysts has been observed by several groups for an oxidative environment.[14,15,35] These studies have often attributed the decay of metal particles to the formation of a volatile metal−adsorbate complex, which results in the disintegration of metal particles. The sintering of supported Au particles induced by O_2 or during CO oxidation cannot be explained simply by the formation of a metal−adsorbate

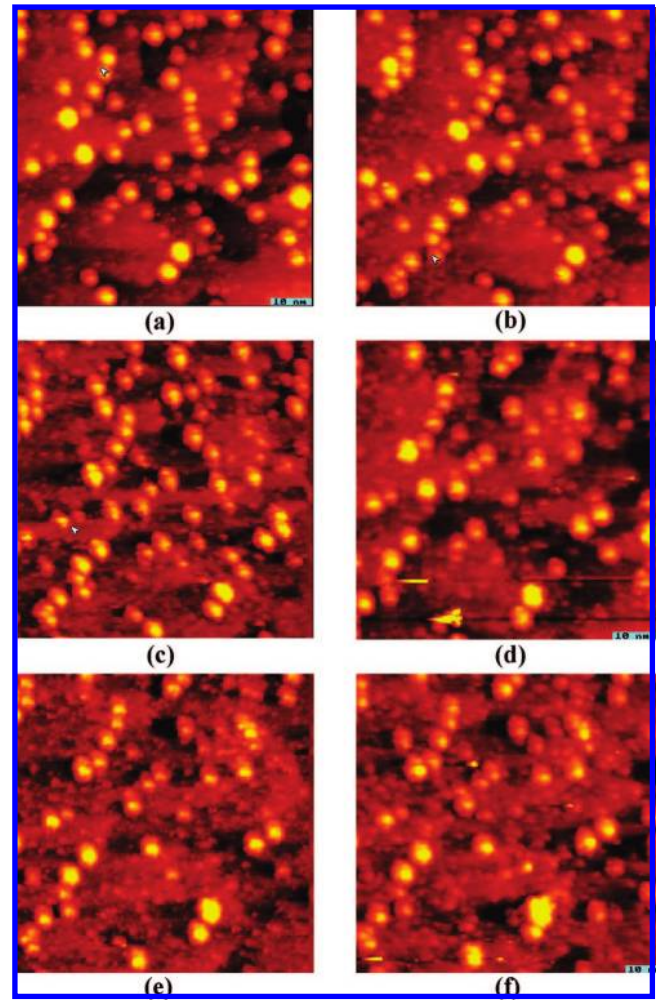

Figure 3. 75 × 75 nm^2 in situ STM images of 0.65 ML Au particles supported on the TiO_2(110) surface in the presence of 0.1 Torr CO and O_2 mixture gas at 410 K. (a−f) STM images subsequently acquired of the same surface region. The time intervals following introduction of the reactants were (a) 0 min; (b) 21 min; (c) 42 min; (d) 63 min; (e) 80 min; and (f) 120 min.

complex. Au particles supported on TiO_2(110) are stable in pure CO gas and have a much slower sintering rate in pure O_2 than when subjected to CO oxidation. If the formation of a metal−oxygen complex gives rise to sintering, then the presence of CO should inhibit the concentration of the metal−oxygen complex and result in a slower rather than an accelerated sintering rate.

Recent STM and density functional theory (DFT) studies suggest that substrate defects play a major role in the stabilization of Au particles.[12,36−40] These studies show that Au particles prefer to nucleate at surface defects such as oxygen vacancies (unsaturated Ti ions) and step edges and that surface defects of TiO_2(110) determine the shape and distribution of Au particles. DFT calculations also show that the binding energy of Au atoms to an oxygen vacancy in TiO_2 is about 1.6 eV. Therefore, the detachment of Au atoms from Au particles must first overcome the interface bonding between the defects and Au. O_2-induced sintering of Au particles supported on TiO_2(110) is likely related to the influence of O_2 on the interface bonding. Various studies have postulated that O_2 adsorbs and dissociates on Au particles or at the interface of Au/TiO_2(110).[11,41−43] Thermodynamically, the adsorption and dissociation of O_2 could heal the surface defect and restrict the interface bonding between the defects and Au. In particular, this effect would destabilize small Au

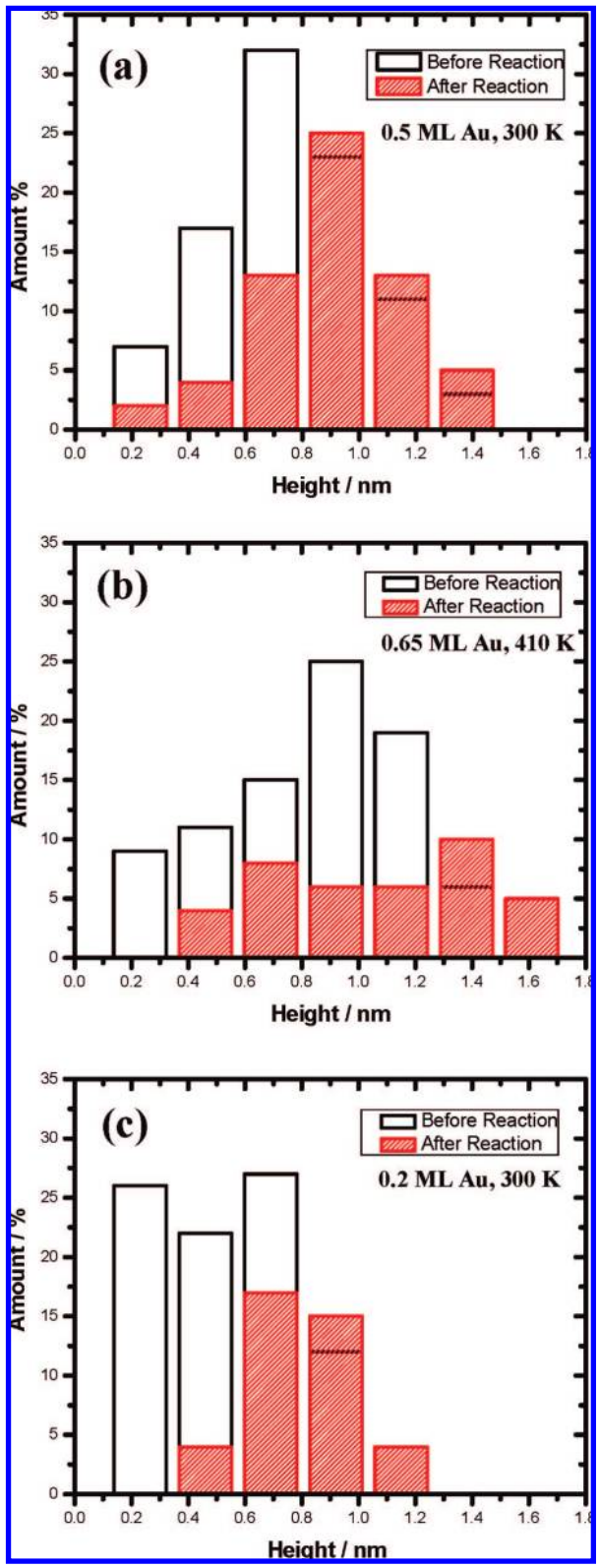

Figure 4. Height distributions of Au particles supported on TiO_2(110) before and after 2 h of CO oxidation (P_{CO}:P_{O2} = 1:1 with the total gas pressure of 0.1 Torr). (a) 0.5 ML, 300 K; (b) 0.65 ML, 410 K; and (c) 0.2 ML, 300 K.

particles due to their low coordination numbers. The stabilization of larger Au particles with a height greater than 4.6 Å is less dependent on the interface bond and thus less influenced by oxygen-induced inhibition of the interface bond.

The synergetic effect of a CO and O_2 mixture might be explained by a reaction-induced mechanism. DFT studies by

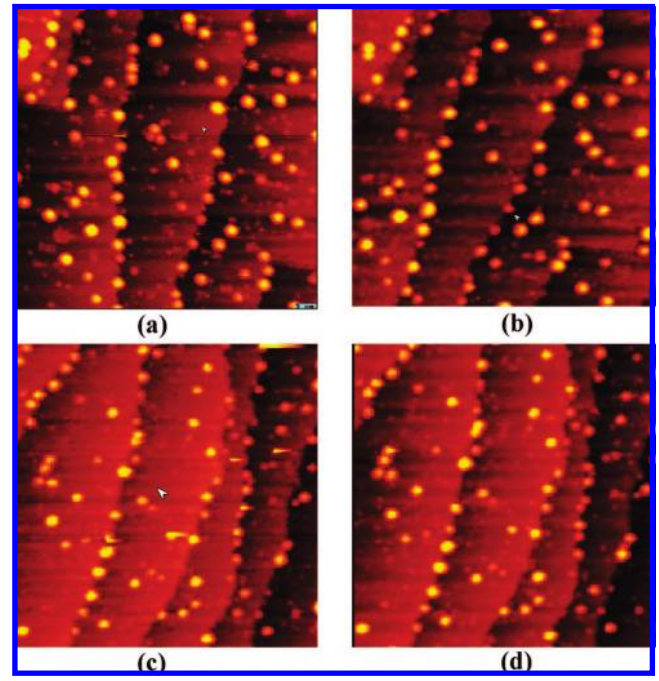

Figure 5. 75 × 75 nm^2 in situ STM images of 0.5 ML Au particles supported on the TiO_2(110) surface in the presence of O_2 or CO. (a) UHV, 300 K; (b) after 1.5 h in 0.1 Torr O_2 at 300 K; (c) UHV, 300 K; and (d) after 2 h in 3 Torr CO at 300 K.

Liu et al.[44] suggest that CO oxidation on Au/TiO_2(110) can proceed with high efficiency without O_2 dissociation. The barrier for the direct bimolecular pathway to produce CO_2 is 0.10 eV, much lower than the dissociation barrier of O_2 on Au/TiO_2(110), 0.52 eV. The production of each CO_2 molecule releases 2.9 eV.[45,46] The energy generated from CO oxidation could very well be transferred to electrons at the surface of the Au particles and excite hot electrons. Ji et al.[45−47] have demonstrated that hot electrons are generated on metal films supported on TiO_2 during CO oxidation. The energy of these hot electrons is larger than the Schottky barrier at the metal−oxide interface (around 0.7−1.2 eV), and the density of hot electrons is found to be proportional to the rate of CO oxidation. It is certainly plausible that hot electrons generated by CO oxidation could induce the detachment of Au monomers from supported Au particles, initiating the sintering process. Indeed, the above sintering kinetic studies yield an activation energy of sintering that tracks the activation energy of CO oxidation on Au/TiO_2, consistent with a reaction-induced sintering mechanism.

The kinetics of sintering can be understood using the Ostwald ripening model developed by Wynblatt and Gjostein[14] (W−J model). The sintering rate equation of supported metal particles was derived on the basis of the steady-state equilibrium of monomers (either metal atoms or metal−adsorbate complex) diffusing across the surface. Recent calorimetric studies by Campbell et al.[48,49] suggest that the free energy of metal nanoparticles is much higher than that conventionally predicted by the Gibbs−Thompson (G−T) relationship. With this correction, the rate equation in W−J model can be rewritten as:

$$\frac{dV_i}{dt} = K \exp\left[-\frac{E_{tot}}{kT}\right]\left[\exp\left(\frac{\mu(r_i^*) - \mu(\infty)}{kT}\right) - \exp\left(\frac{\mu(r_i) - \mu(\infty)}{kT}\right)\right]$$

where V_i is the volume of particle i, K is the prefactor dependent on the controlling kinetic process of diffusion, E_{tot} is the total

activation energy for bulk metal, $\mu(r_i)$ is the chemical potential (partial molar free energy) of the particle i with radius of r_i, and $\mu(\infty)$ is the chemical potential of the bulk metal. Here, r_i^* is the critical radius of the particle that neither decays nor grows at diffusion equilibrium. Assuming particles on the surface are in equilibrium with the same far field monomer concentration (mean-field approximation), r_i^* is the average radii of all particles and increases as a function of time during the sintering. Particles with radii smaller than r_i^* will decay, whereas particles with radii larger than r_i^* will grow. Their sintering rates depend on their chemical potentials, as well as the chemical potential of $\mu(r_i^*)$.

The chemical potential of metal particles decreases as their radii increase. Higher surface particle coverage will in general result in a higher r_i^* and thus a smaller $\mu(r_i^*)$. The decay rates for particles with radii smaller than r_i^* increase with a decrease of $\mu(r_i^*)$. Thus, the decay rates of Au particles smaller than r_i^* increase with the surface coverage. For supported metal particles with positive activation energies, the rate of sintering will increase as the surface temperature increases.

In the sintering rate equation, the prefactor K depends on the process that limits the kinetics of sintering. Two limiting kinetic processes are described in the W−J model, interface control and diffusion control. In the interface control limit, where the detachment of monomers from particles is the rate-limiting step, K is only a function of particle radius. As the distance between particles increases and mass transport becomes more and more dependent on the surface diffusion of monomers, K becomes a function of particle radius as well as the diffusion length of the monomers. When the distance between particles is larger than the diffusion length, at which the surface concentration of monomers reaches a far field minimum, the rate equation becomes diffusion limited.

In the above kinetic studies of sintering, the number density decreases and becomes constant around $7 \times 10^{11}/\mathrm{cm}^2$, independent of the surface Au coverage or temperature. The constant number density of Au particles exhibits a drastic decrease in sintering rates at the later stage of sintering. The independence of particle number density to surface coverage and temperature further suggests that, instead of particle radius or temperature, the increased distance between particles might account for the decreased sintering rate at the later stage of sintering. Because the critical radius r_i^* increases as a function of time, the disappearance of particles of certain radius, smaller than r_i^*, is an accelerated process when the sintering process is simply limited by the interface reaction. In the above studies of different Au coverages, the decrease of small Au particles always slows when the number density is reduced to $7 \times 10^{11}/\mathrm{cm}^2$, or a mean interparticle distance of 12 nm. The decreased sintering rate suggests surface diffusion becomes critical in the later stage of sintering.

Size-dependent activation energies of sintering can be extrapolated for particles of different radius by analyzing the sintering rates of individual particles. Small Au particles, with heights around 4.6 Å or less, exhibit similar decay rates at the same temperature. However, intermediate-sized Au particles, with heights near the median height of the particle distribution, show various sintering rates depending on their local particle configuration. For example, for the sintering of 0.5 ML Au/TiO_2(110) at 300 K, particles of similar height and diameter (0.7−0.9 nm in height and ∼4 nm in diameter, marked by dashed circles in Figure 1) sinter at different rates. Within different regions of the surface, the kinetics of sintering can vary. Depending on the size of neighboring particles, a larger particle (e.g., particle a in Figure 1) can decay, while a smaller particle (e.g., particle b in Figure 1) can grow in different local environments.

In the W−J model, the mean-field approximation enables the rate equation of sintering to be applied to all particles on the surface. With this approximation, for a certain model system at constant temperature, the rate equation gives the same sintering rate for particles of the same radius. The above behavior cannot be understood by the mean-field approximation but can be explained by the differences in size and position of particles in the local vicinity, that is, the local effect. Indeed, the breakdown of the mean-field approximation most likely occurs for real systems because long-range equilibrium can only exist in the two kinetic limits described in the W−J model. Deviations from these limits lead to gradients in the monomer density and thus to local effects. Meanwhile, structural defects such as step edges or large diffusion barriers break the diffusion equilibrium across the surface. The decay or growth rate of an individual particle is thus decided by the location and size of neighboring particles.

The failure of the mean-field approximation was previously observed in the thermal ripening of 2D islands on both metal and Si surfaces in UHV;[50−53] that is, local effects dominate Ostwald ripening. A simplified analytical approach, "nearest neighbor approach", has been proposed to extrapolate the controlling kinetic parameters, assuming the sintering of a particle is decided by nearest neighboring particles.[51−55] Mathematically, all particles on the surface could be simulated by the W−J model; however, for each particle, r_i^* varies with the spatial configuration of its neighboring particles. For particles of the same size, the tendency or rate of sintering can be different depending on whether there are neighboring particles with larger or smaller r_i^* in their local environment. The dominance of local effects is expected to cause the broadening of size distribution and lead to the deviation between the mean-field based simulation and experimental data.

For Au particles with a height of 4.6 Å or less, their decay rates are rapid and less dependent on the local spatial configuration of Au particles. The lack of dependence of the decay rates on the local environments is due to the large difference of chemical potentials between small particles and particles with radii of r_i^*. Because the chemical potential of particles increases steeply in the range of nanometer size, the chemical potential difference between particles of different sizes could lead to $e^{\mu(r_i^*)-\mu(\infty)/kT} \ll e^{\mu(r_i)-\mu(\infty)/kT}$; that is, the sintering rates of supported metal particles are determined only by their own chemical potentials, but not their neighbors when the particles are sufficiently smaller than r_i^*. Therefore, the rate equation for small particles is mainly determined by the monomer concentration near the particle and can be simplified as:

$$\frac{\mathrm{d}V_i}{\mathrm{d}t} = -K \exp\left[-\frac{E_{\mathrm{tot}} - [\mu(r_i) - \mu(\infty)]}{kT}\right]$$

The decay rate of small particles is independent of r_i^* and thus the local particle distribution. This simplification is justified on the basis of theoretical models of the chemical potentials of Au particles supported on TiO_2(110). A modified pairwise bond-additivity (MBA) model has been proposed by Campbell et al. with consideration of the low coordination number of nanoparticles.[16,49] Taking into account the influence of surface defects, Lopez et al.[39] have proposed an equation to calculate the chemical potential of Au particles supported on a TiO_2(110) surface. From either of these models (Figure 6), the difference of the chemical potentials between particles with size close to the critical radius (diameters around 4−5 nm) and small particles

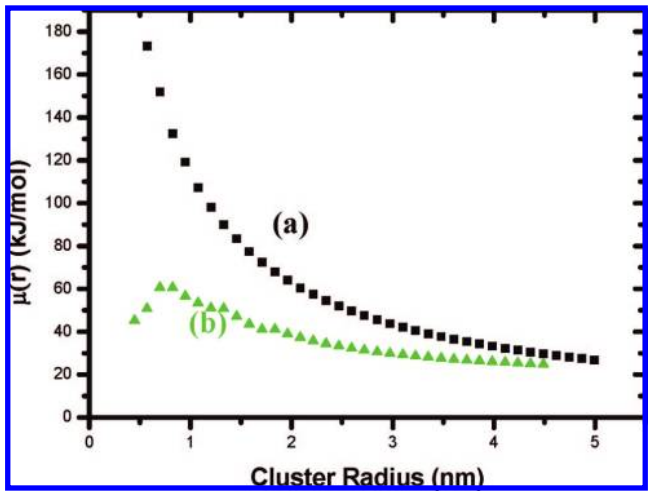

Figure 6. Calculated free energies of Au particles supported on TiO_2(110) based on (a) MBA model; and (b) model by Lopez et al. including surface defects. In this calculation, the aspect ratio of Au particles was determined on the basis of STM measurements. In (b), the number of defects under each Au particle is set at $n = 9$ for Au particles of all size. Assuming 10% surface defects, $n = 9$ corresponds to the number of defects under Au particles of 2.4 nm radius. For supported Au particles with radius smaller than 2.4 nm, the free energy of Au particles could be much higher with reduced surface defects.

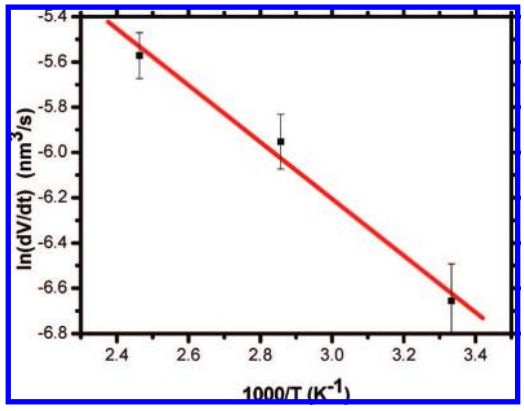

Figure 7. Arrhenius plot for the decay of nanoparticles. ln(dV/dt) is estimated from the average decay rates of particles with a diameter around 3 nm. The solid line reflects the best least-squares fit to the data.

(diameters around 3 nm) always satisfies $[\mu(r_i^*) - \mu(\infty)] - [\mu(r_i) - \mu(\infty)] < -10$ kJ/mol, leading to $e^{\mu(r_i^*)-\mu(\infty)/kT} \ll e^{\mu(r_i)-\mu(\infty)/kT}$. For small Au particles, the rate equation can be simplified as

$$\frac{dV_i}{dt} = -K \exp\left[-\frac{E_{tot} - [\mu(r_i) - \mu(\infty)]}{kT}\right]$$

Therefore, for small Au particles, a plot of ln(dV_i/dt) versus 1/T gives the activation energy of sintering as $E_{tot} - [\mu(r_i) - \mu(\infty)]$. The volume of Au particles during CO oxidation can be calculated using the volume equation for a spherical cap, $V = {}^1/_6\pi h(3r^2 + h^2)$, where r and h are the radius and height of clusters measured from the STM images. As shown in Figure 7, the activation energy for Au particles with diameters around 3 nm is 10 ± 2 kJ/mol. Previous studies have shown a size-dependent reactivity in CO oxidation, and the apparent activation energy of CO oxidation is 14 kJ/mol for Au particles with an average diameter of 3 nm supported on the TiO_2(110).[56] Because the apparent activation energy of CO oxidation is an average value for Au particles with a size distribution, the actual apparent activation energy can be lower for Au particles of 3 nm size. Therefore, the activation energy of sintering tracks closely the activation energy of CO oxidation on supported Au particles.

Campbell et al. estimated the activation energy of sintering for Au particles supported on TiO_2(110) in UHV.[16,49] The activation energy for Au particles with diameters around 3 nm was ~280 kJ/mol (E_{tot} = 327 kJ/mol and $\mu(r) - \mu(\infty) \approx 50$ kJ/mol). The large difference in the activation energy of sintering between UHV and during CO oxidation demonstrates the influence of CO oxidation on particle sintering. This effect very well may be general for CO oxidation over other supported metal catalysts.

Conclusions

In summary, we have studied CO oxidation-induced sintering of Au particles supported on TiO_2(110), and we measured the sintering kinetics of individual particles in the presence of 0.1 Torr O_2 or CO/O_2 mixture. By comparing the sintering rates of Au particles in the presence of different reactants, a reaction-induced and accelerated sintering process is observed. Through real time measurements, we conclude that Au particles sinter via Ostwald ripening in the presence of O_2 or a CO/O_2 mixture at temperatures between 300 and 410 K. The sintering of Au particles supported on TiO_2(110) does not follow the mean-field assumption due to significant local effects. The activation energy of sintering for Au particles around 3 nm correlates with the activation energy of CO oxidation and is consistent with a reaction-induced mechanism.

Acknowledgment. We gratefully acknowledge the support for this work by the Department of Energy (DOE), Office of Basic Energy Sciences, Division of Chemical Sciences, under grant number DE-FG02-95ER14511 and by the Robert A. Welch Foundation.

References and Notes

(1) Corti, C. W.; Holliday, R. J.; Thompson, D. T. *Top. Catal.* **2007**, *44*, 331–343.
(2) Bond, G. C.; Thompson, D. T. *Catal. Rev.-Sci. Eng.* **1999**, *41*, 319–388.
(3) Freund, H. J.; Baumer, M.; Kuhlenbeck, H. *Adv. Catal.* **2000**, *45*, 333–384.
(4) Henry, C. R. *Surf. Sci. Rep.* **1998**, *31*, 235–325.
(5) Campbell, C. T. *Surf. Sci. Rep.* **1997**, *27*, 1–112.
(6) Campbell, C. T.; Grant, A. W.; Starr, D. E.; Parker, S. C.; Bondzie, V. A. *Top. Catal.* **2001**, *14*, 43–51.
(7) Bartholomew, C. H. *Stud. Surf. Sci. Catal.* **1997**, *111*, 585–592.
(8) Haruta, M.; Date, M. *Appl. Catal., A* **2001**, *222*, 427–437.
(9) Valden, M.; Lai, X.; Goodman, D. W. *Science* **1998**, *281*, 1647–1650.
(10) Rainer, D. R.; Goodman, D. W. *J. Mol. Catal. A* **1998**, *131*, 259–283.
(11) Haruta, M. *Catal. Today* **1997**, *36*, 153–166.
(12) Lai, X.; St. Clair, T. P.; Valden, M.; Goodman, D. W. *Prog. Surf. Sci.* **1998**, *59*, 25–52.
(13) Chakraverty, B. K. *J. Phys. Chem. Solids* **1967**, *28*, 2401–2412.
(14) Wynblatt, P.; Gjostein, N. A. *Prog. Solid State Chem.* **1975**, *9*, 21–58.
(15) (a) Harris, P. J. F. *Int. Mater. Rev.* **1995**, *40*, 97–115. (b) Datye, A. K.; Xu, Q.; Kharos, K. C.; McCarty, J. M. *Catal. Today* **2006**, *111*, 59–67.
(16) Campbell, C. T.; Parker, S. C.; Starr, D. E. *Science* **2002**, *298*, 811–814.
(17) (a) Kolmakov, A.; Goodman, D. W. *Catal. Lett.* **2000**, *70*, 93–97. (b) Starr, D. E.; Shaikhutdinov, S. K.; Freund, H. J. *Top. Catal.* **2005**, *36*, 33–41.
(18) Kolmakov, A.; Goodman, D. W. *Surf. Sci.* **2001**, *490*, L597−L601.
(19) Kolmakov, A.; Goodman, D. W. *Chem. Rec.* **2002**, *2*, 446–457.
(20) Santra, A. K.; Kolmakov, A.; Yang, F.; Goodman, D. W. *Jpn. J. Appl. Phys.* **2003**, *42*, 4795–4798.
(21) Cosandey, F.; Madey, T. E. *Surf. Rev. Lett.* **2001**, *8*, 73–93.
(22) Smith, R. D.; Bennett, R. A.; Bowker, M. *Phys. Rev. B* **2002**, *66*, 035409.

(23) Onishi, H.; Iwasawa, Y. *Phys. Rev. Lett.* **1996**, *76*, 791–794.
(24) Lai, X. F.; St. Clair, T. P.; Goodman, D. W. *Faraday Discuss.* **1999**, *114*, 279–284.
(25) Zhou, J.; Kang, Y. C.; Ma, S.; Chen, D. A. *Surf. Sci.* **2004**, *562*, 113–127.
(26) Zhou, J.; Kang, Y. C.; Chen, D. A. *J. Phys. Chem. B* **2003**, *107*, 6664–6667.
(27) Kielbassa, S.; Habich, A.; Schnaidt, J.; Bansmann, J.; Weigl, F.; Boyen, H. G.; Ziemann, P.; Behm, R. J. *Langmuir* **2006**, *22*, 7873–7880.
(28) Kielbassa, S.; Kinne, M.; Behm, R. J. *J. Phys. Chem. B* **2004**, *108*, 19184–19190.
(29) Berko, A.; Menesi, G.; Solymosi, F. *J. Phys. Chem.* **1996**, *100*, 17732–17734.
(30) Berko, A.; Solymosi, F. *Surf. Sci.* **1998**, *411*, L900−L903.
(31) Diebold, U. *Surf. Sci. Rep.* **2003**, *48*, 53–229.
(32) Berko, A.; Solymosi, F. *J. Catal.* **1999**, *183*, 91–101.
(33) Berko, A.; Solymosi, F. *J. Phys. Chem. B* **2000**, *104*, 10215–10221.
(34) Berko, A.; Szoko, J.; Solymosi, F. *Surf. Sci.* **2004**, *566*, 337–342.
(35) Bartholomew, C. H. *Stud. Surf. Sci. Catal.* **1997**, *111*, 585–592.
(36) Chen, M. S.; Goodman, D. W. *Acc. Chem. Res.* **2006**, *39*, 739–746.
(37) Chen, M. S.; Goodman, D. W. *Science* **2004**, *306*, 252–255.
(38) Wahlstrom, E.; Lopez, N.; Schaub, R.; Thostrup, P.; Ronnau, A.; Africh, C.; Laegsgaard, E.; Norskov, J. K.; Besenbacher, F. *Phys. Rev. Lett.* **2003**, *90*, 26101.
(39) Lopez, N.; Norskov, J. K.; Janssens, T. V. W.; Carlsson, A.; Puig-Molina, A.; Clausen, B. S.; Grunwaldt, J. D. *J. Catal.* **2004**, *225*, 86–94.
(40) Santra, A. K.; Yang, F.; Goodman, D. W. *Surf. Sci.* **2004**, *548*, 324–332.
(41) Grunwaldt, J. D.; Baiker, A. *J. Phys. Chem. B* **1999**, *103*, 1002–1012.
(42) Bondzie, V. A.; Parker, S. C.; Campbell, C. T. *Catal. Lett.* **1999**, *63*, 143–151.
(43) Bollinger, M. A.; Vannice, M. A. *Appl. Catal., B* **1996**, *8*, 417–443.
(44) Liu, Z. P.; Gong, X. Q.; Kohanoff, J.; Sanchez, C.; Hu, P. *Phys. Rev. Lett.* **2003**, *91*, 266102.
(45) Ji, X. Z.; Zuppero, A.; Gidwani, J. M.; Somorjai, G. A. *J. Am. Chem. Soc.* **2005**, *127*, 5792–5793.
(46) Ji, X. Z.; Somorjai, G. A. *J. Phys. Chem. B* **2005**, *109*, 22530–22535.
(47) Ji, X. Z.; Zuppero, A.; Gidwani, J. M.; Somorjai, G. A. *Nano Lett.* **2005**, *5*, 753–756.
(48) Starr, D. E.; Ranney, J. T.; Larsen, J. H.; Musgrove, J. E.; Campbell, C. T. *Phys. Rev. Lett.* **2001**, *87*, 106102.
(49) (a) Parker, S. C.; Campbell, C. T. *Phys. Rev. B* **2007**, *75*, 035430. (b) Parker, S. C.; Campbell, C. T. *Top. Catal.* **2007**, *44*, 3–13.
(50) Rosenfeld, G.; Morgenstern, K.; Beckmann, I.; Wulfhekel, W; Leagsgaard, E.; Besenbacher, F.; Comsa, G. *Surf. Sci.* **1998**, *402−404*, 401–408.
(51) Morgenstern, K.; Rosenfeld, G.; Comsa, G.; Sorensen, M. R.; Hammer, B.; Laegsgaard, E.; Besenbacher, F. *Phys. Rev. B* **2001**, *63*, 045412.
(52) Bartelt, N. C.; Theis, W.; Tromp, R. M. *Phys. Rev. B* **1996**, *54*, 11741–11751.
(53) Theis, W.; Bartelt, N. C.; Tromp, R. M. *Phys. Rev. Lett.* **1995**, *75*, 3328–3331.
(54) Morgenstern, K.; Rosenfeld, G.; Comsa, G. *Surf. Sci.* **1999**, *441*, 289–300.
(55) Rosenfeld, G.; Morgenstern, K.; Esser, M.; Comsa, G. *Appl. Phys. A* **1999**, *69*, 489–496.
(56) Valden, M.; Pak, S.; Lai, X.; Goodman, D. W. *Catal. Lett.* **1998**, *56*, 7–10.

JP807865W